JOURNAL OF MATERIALS SCIENCE 28 (1993) 3885–3894

Semi-solid deformation in multi-component nickel aluminide

Part II *Directionally solidified alloys*

C.S. LIN and J.A. SEKHAR
Department of Materials Science and Engineering, International Centre for Micropyretics, University of Cincinnati, Cincinnati, OH 45221, USA

A systematic study was carried out to determine the solidification and the tensile behaviour of semi-solid multicomponent nickel aluminide. Directionally solidified samples were tested at various temperatures in the mushy (semi-solid) region. A special Gleeble testing procedure was developed where transverse and longitudinal (5 mm) samples were quickly raised to a predetermined temperature in the semi-solid zone and fractured. The fracture stresses were found to decrease monotonically with temperature. The strain to fracture exhibited a ductility minimum at an intermediate temperature in the semi-solid zone. The effect of the solidification process variables, namely, the temperature gradient and velocity, on the fracture stress in the transverse direction was to increase the fracture stress at a given temperature. In the longitudinal direction, the fracture stress decreases with the temperature gradient and was relatively independent of velocity. At the temperature corresponding to the strain minimum, residual microcracks were detected on the fracture surface. The upper hot tearing temperature was noted to be a function of the solidification variables. The amount of strain accommodation and the hot tearing resistance was found to be influenced by the solidification microstructure. Fracture maps which include the transverse fracture stress, temperature, and temperature gradient during solidification (σ_T–T–G) for the directionally solidified microstructures are presented. A castability map is created from the fracture data.

1. Introduction

Although hot tearing in directionally solidified structures is not as severe a problem as hot tearing in equiaxed structures, examples exist where hot tearing has been known to limit the processing of alloys during directional solidification, especially when section size issues become important. In addition, a positive temperature gradient is always present during directional solidification which may impose thermal stresses during solidification. In this study, we examine the effect of the solidification variables, namely, the temperature gradient, G, and the velocity, V, on the mechanical properties of the mushy zone during the directional solidification of IC396M. The composition of IC396M is given in Part I [1] of this study.

In this study, carefully solidified directional microstructures were tested for strength at various temperatures in the semi-solid range. The samples were obtained from studies reported previously [2, 3] which were aimed at understanding residual solidification microporosity. For this, all the relevant dendrite scales were carefully recorded and correlated with residual microporosity [2, 3]. Thus, the samples were well characterized prior to testing in the semi-solid state. In addition, the samples possessed microporosity associated with the primary γ' which presumably prevented any problems associated with the initiation of microcracking. In this article, the onset of microcracking is discussed from observations of the strain to fracture. Residual microcracking in solidified structures is also critically examined.

All the directionally solidified samples were either single crystals or contained, at the most, a single grain boundary. Thus, the results on fracture strain and stress could be correlated to the dendrite parameters.

2. Experimental technique

The strength in the semi-solid zone was measured with a Gleeble unit (a thermomechanical testing device; Duffers Scientific) as discussed in Part I [1]. Samples of IC396M grown under different conditions [2, 3] were cut both longitudinally (i.e. parallel to heat flow) and transversely (i.e. perpendicular to heat flow) and shaped as shown in Fig. 1 of Part I [1]. Table I shows the conditions, including the temperature gradient and growth velocity for the samples studied in this paper. The experimental details of Gleeble testing have been discussed in Part I [1] of this paper.

One of the directionally solidified samples, solidified at a temperature gradient of $G = 5.4\ \mathrm{K\,mm^{-1}}$, and a velocity of $V = 191.5\ \mu\mathrm{m\,s^{-1}}$, was heated in the

0022–2461

Gleeble until it attained a temperature of 1600 K in the centre region and was then quenched by shutting off the current. Seven K-type thermocouples were used to control the heating rate and to record the actual temperature profile during cooling. Similar measurements were made in all the test samples at the two points. The gradient during cooling, measured in all the samples, was of the order of 10 K mm^{-1} near the mid-section but could increase to over 100 K mm^{-1} near the jaws and was a function of the testing parameters, including the exact length of specimen and the efficiency of thermal contact with the jaws. The rate of reheating to the desired temperature was approximately 20 K s^{-1}. The fracture surface always intersected the plane containing the thermocouple bead (i.e. the mid-point of the gauge). We therefore estimate our results to have a $\pm$ 5 K accuracy by assuming that the maximum deviation of the fracture plane from the position of the bead was no more than 0.5 mm.

Gleeble testing of the IC396M samples as shown in Part I [1] (with water-cooled ends for gripping) was performed at various temperatures with an argon cover. The local temperature along the fracture line was measured with a K-type thermocouple which was spot welded to the specimen. Continuous temperature recording was made during the test.

3. Results and discussion

3.1. Stress–strain relationship in the semi-solid zone

Stress–strain relationships were obtained with the Gleeble at temperatures ranging from 1300–1543 K for the directionally solidified microstructures. The lower temperature was lower than the lowest melting eutectic in the alloy [2] and the higher temperature was the temperature at which the alloy developed no strength. A typical relationship is shown in Fig. 1. The temperature at which the first liquid film was seen is discussed in Section 3.2. We note, however, that, as before [4], the as-directionally solidified materials possess higher strength than the worked materials at temperatures where no liquid phase was present. However, as soon as a liquid phase appeared (i.e. at temperature > 1360 K for the as-solidified directional material) the strength of the directly solidified sample was noted to fall to levels lower than the worked sample. Table II shows the measured modulus as a function of the temperature and solidification variables for the samples tested in this study.

3.2. Fracture in directionally solidified alloys

3.2.1. Stress

From the plot of the stress–temperature measurements (Fig. 2) it was noted that the strength measured along the longitudinal direction of the microstructure was always greater than the transverse direction. The reason for this may be as follows. At the test temperatures, the regions between the dendrites will be partially molten. When the samples are tested in the transverse direction, the fracture occurs in the weak

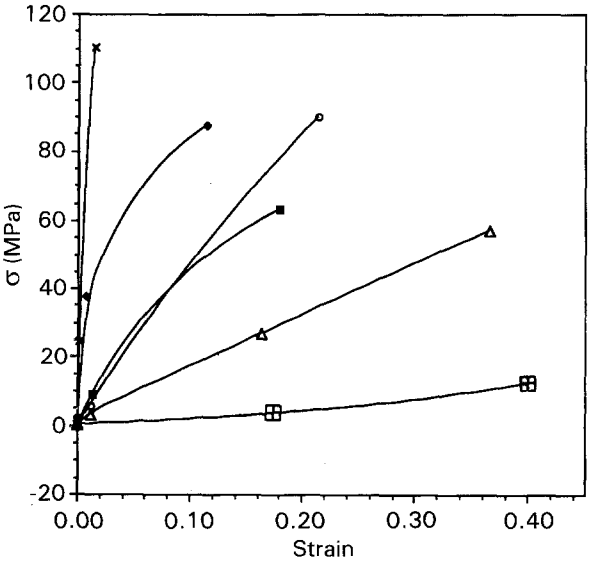

Figure 1 Stress–strain relationship for directionally solidified microstructure, $G = 20$ K mm^{-1}, $V = 17.9$ μm s^{-1}. (⊠) 1470 K, (△) 1400 K, (■) 1378 K, (◆) 1359 K, (○) 1326 K, (×) 1303 K.

TABLE I Conditions for directional solidification

Velocity, V (μm s^{-1})	Temperature gradient, G, (K mm^{-1})
6.0	20
17.9	20
26.1	20
6.8	9
17.0	9
25.9	9
120.0	9
4.3	5.4
16.8	5.4
191.5	5.4

interdendritic regions and there may be no continuous solid to take up the load further, i.e. the solid and liquid are in a series-type configuration. However, some weak solid bridges (leading to frictional constraints) may be present, arising primarily from the weak interconnection of secondary dendrites. This bridge is expected to disappear progressively as the testing temperature is raised.

In the longitudinal direction, the cross-section contains both continuous dendrites and nearly continuous interdendritic regions. The deformation therefore involves fracture of both the dendrites and the interdendritic region (i.e. the solid and liquid are in a parallel-type configuration). Hence, higher strengths may be expected in the longitudinal direction as the solid section takes up a larger part of the load. The transverse and longitudinal fracture stresses approach the same value as the testing temperature is increased (Fig. 2). At the higher temperatures, the dendrites melt and the continuity of solid bridging in the longitudinal direction begins to disappear.

The temperature at which the fracture stress becomes very small is higher for the longitudinal section when compared to the transverse section. Additionally, it is noted that the solidification variables may

TABLE II Measured mushy zone properties from stress-free directionally solidified samples. σ_f is the fracture stress at the same temperature. The modulus, E_T, is determined from the average slope between the first two or three data points of the type shown in Fig. 1. This modulus may somewhat underestimate the slope at the origin

G (K mm^{-1})	V(μm s^{-1})	T (K)	E (MPa)	σ_f, (MPa)
5.4	4.3	1413	171.53	2.48
		1391	7.89	2.78
		1364	711.98	26.08
		1362	2966.7	28.82
		1336	942.71	37.62
	16.8	1423	0.82	3.30
		1398	1325.9	26.52
		1366	834.69	40.16
		1315	930.23	80.34
	191.5	1539	590.75	24.17
		1443	356.65	41.93
		1366	611.29	50.71
		1352	1567.0	131.1
9	6.8	1465	12.600	3.91
		1421	59.520	10.08
		1375	714.28	21.54
		1349	963.00	36.16
	25.9	1475	6.46	2.08
		1422	328.91	23.19
		1365	3055.1	50.25
		1317	540.10	99.39
20	6.0	1481	10.99	5.06
		1420	494.65	17.12
		1369	148.03	24.68
		1367	445.00	26.79
	17.9	1470	5.14	12.27
		1400	16.25	57.08
		1378	61.25	63.28
		1359	4200.0	87.37
		1326	500.00	89.87
		1303	1100.0	110.5

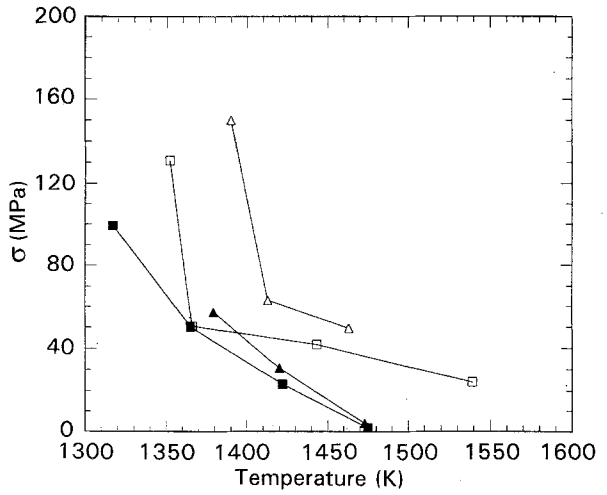

Figure 2 The (▲, △) longitudinal and (■, □) transverse maximum engineering stress at failure versus temperature for directionally solidified IC396M at (■, ▲) $G = 9$ K mm^{-1}, $V = 25.9$ μm s^{-1} and (□, △) $G = 5.4$ K mm^{-1}, $V = 191.5$ μm s^{-1}.

influence this temperature significantly. This temperature is the upper hot tearing temperature and is noted to be a function of the imposed solidification variables which control the morphology of growth. For example, the upper hot-tearing temperature increases with the temperature gradient, G, imposed

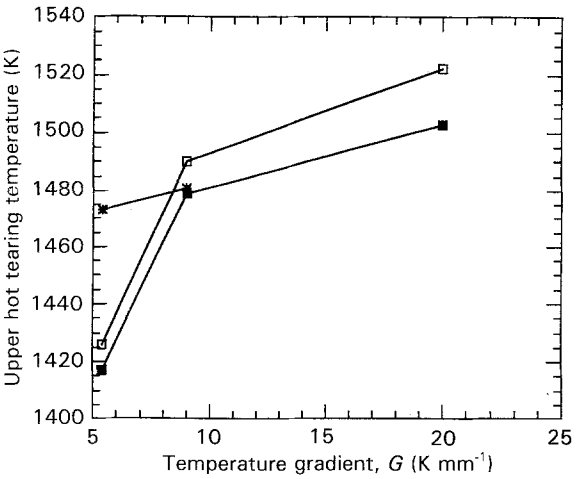

Figure 3 Upper hot tearing temperature versus temperature gradient for directionally solidified IC396M. (■) Transverse, $V \simeq 6$ μm s^{-1}; (□) transverse, $V = 20$ μm s^{-1}; (*) longitudinal, $V \simeq 6$ μm s^{-1}.

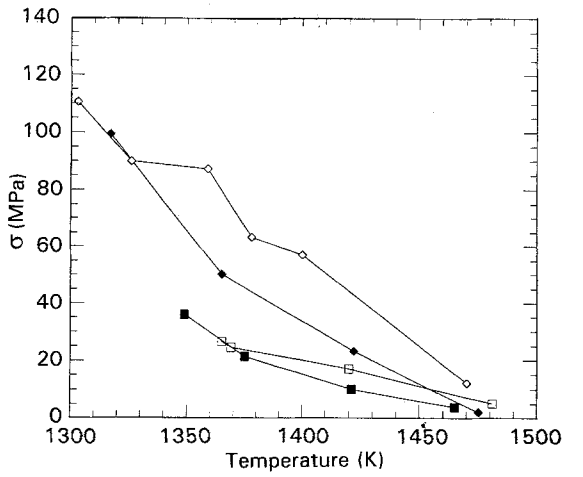

Figure 4 The transverse engineering stress to failure versus temperature for the same temperature gradient, $G = 20$ K mm^{-1} for velocities, $V = (\diamond)$ 17.9, (□) 6.0 μm s^{-1}, and $G = 9$ K mm^{-1} for $V = (\blacklozenge)$ 25.9 and 6.8 (■) μm s^{-1}.

during solidification (Fig. 3). The upper hot-tearing temperature is noted to be relatively insensitive to the solidification velocity in the range 1–20 μm s^{-1} but then increases in the range 20–200 μm s^{-1}. The fracture stress continuously falls with increasing testing temperature. An approximate measure of the stress, σ_f, is given by $\sigma_f = 2\gamma_{lv}/d$ [5], where d is the film thickness and γ_{lv} is the liquid–vapour interfacial energy.

As the velocity of solidification increases, the measured transverse fracture stress at a given testing temperature is noted to increase (Figs 4, 5). However, the longitudinal stress is relatively insensitive to the solidification velocity. As the solidification velocity increases, the secondary arm spacing, λ_2, decreases in the IC396M [2] alloy. For transverse testing, this may imply higher frictional forces during deformation, and an increase in the strength with increasing solidification velocity. Fig. 6 is a plot of the secondary arm spacing and transverse strength. A correlation is apparent which shows the transverse stress falling with increasing λ_2. In the case of longitudinal testing, the

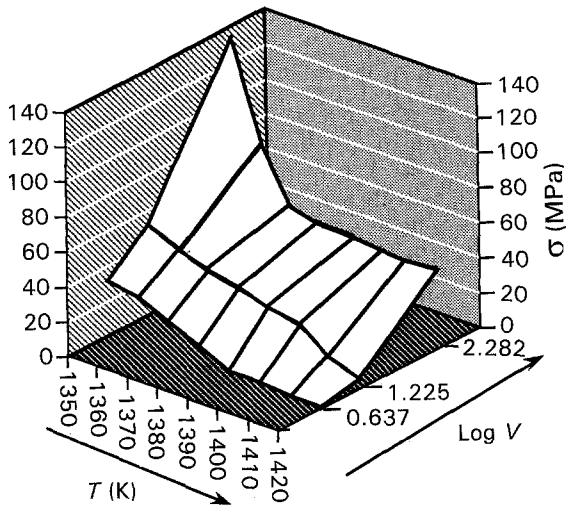

Figure 5 The transverse engineering stress to failure versus temperature for the same temperature gradient, $G = 5.4\,\mathrm{K\,mm^{-1}}$, for various velocities, $V = 4.3, 16.8, 191.5\,\mu\mathrm{m\,s^{-1}}$.

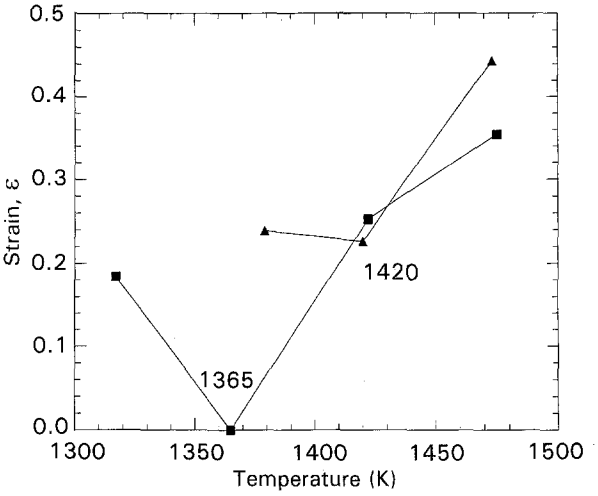

Figure 7 The (▲) longitudinal and (■) transverse strain at failure, ε, versus temperature, T, for directionally solidified IC396M. Conditions of solidification are $G = 9\,\mathrm{K\,mm^{-1}}$, $V = 25.9\,\mu\mathrm{m\,s^{-1}}$. The temperatures marked in the figure are the minima temperatures.

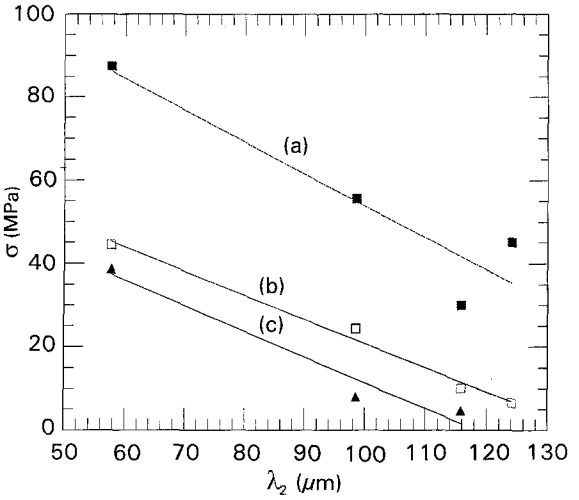

Figure 6 The transverse engineering stress at failure versus the secondary dendrite arm spacing for temperatures, (■) 1360, (□) 1420 and (▲) 1460 K. (a) $y = 130.38 + -0.76561x$, $R = 0.93173$. (b) $y = 78.552 + -0.57742x$, $R = 0.99413$. (c) $y = 72.843 + -0.61476x$, $R = 0.97894$.

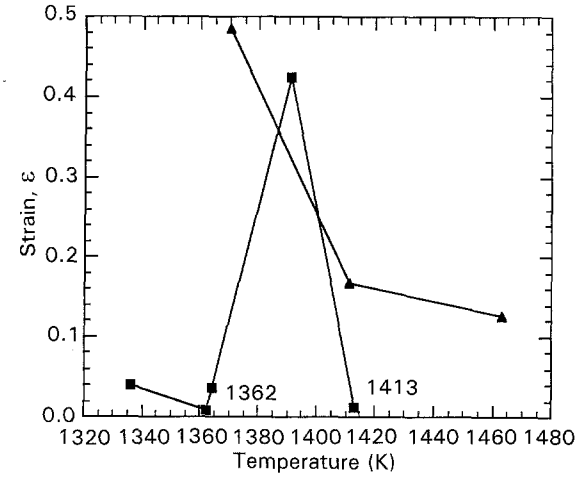

Figure 8 The (▲) longitudinal and (■) transverse strain at failure, ε, versus temperature, T, for directionally solidified IC396M. Conditions of solidification are $G = 5.4\,\mathrm{K\,mm^{-1}}$, $V = 4.3\,\mu\mathrm{m\,s^{-1}}$. The temperatures marked in the figure are the minima temperatures.

primary dendrite arm spacing, λ_1, in IC396M is only weakly affected by velocity [2]. If the primary spacing influences the longitudinal strength, then this is a possible reason for the insensitivity to velocity. We do not, however, find any clear, direct correlation between λ_1 and fracture stress, σ_f (both transverse and longitudinal). The longitudinal fracture stress shows an initial decrease and then an increase as a function of λ_2. The minimum of the longitudinal fracture stress was always noted to occur at $\lambda_2 = 100\,\mu\mathrm{m}$ for all of the temperatures tested.

3.2.2. Strain

In the plot of strain at failure, ε, versus temperature, T, a ductility minimum may often be encountered (Figs 7, 8). This often occurs at a temperature truely lower than the upper hot tearing temperature. The strain at this minimum, $\varepsilon_{\mathrm{min\ f}}$, is often zero or close to zero, especially for transverse testing. At $T\varepsilon_{\mathrm{min\ f}}$ (i.e. the temperature at which the strain minimum occurs), a thin interconnected liquid film may appear which allows for crack propagation during tensile deformation without the possibility of blunting the crack or reducing the crack length by the collapse of the adjacent liquid. A typical solidified film-like residue is noted on the fracture surface and is shown in Fig. 9. This micrograph was taken from a sample fractured at the ductility minimum. The thin, film-like residue is surrounded by dendrites from resolidified liquid. The dendrite arm spacing of the resolidified liquid ($\sim 4\,\mu\mathrm{m}$) is much smaller than that of the original cast dendrites ($> 50\,\mathrm{mm}$). Energy dispersive X-ray analysis (EDAX) of the thin film showed that the region contained iron, whereas no iron was detected in the other regions of the fractographs. The films appeared to be featureless.

At temperatures below the ductility minimum, the liquid-film residue was not in evidence. Thus, some ductility was observed. At temperatures higher than

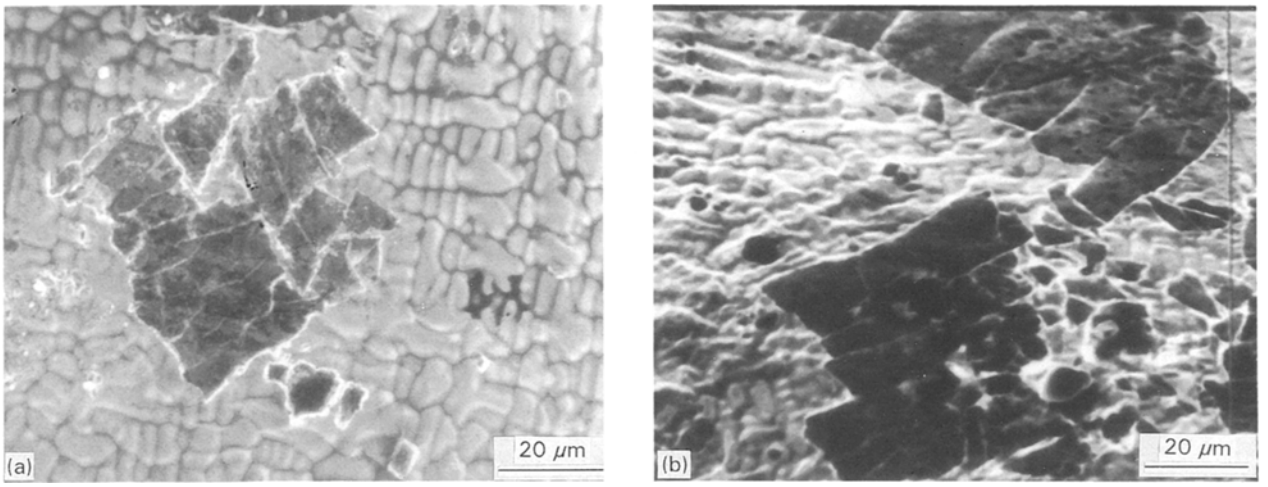

Figure 9 A typical film residue in the transverse scanning electron microscope fractograph of an elevated temperature fracture produced at (a) 1359 K (in argon) for the directionally solidified sample at $G = 20\ \mathrm{K\,mm^{-1}}$ and $V = 17.9\ \mu\mathrm{m\,s^{-1}}$; (b) 1362 K (in argon) for the equiaxed solidified at cooling rate $0.5\ \mathrm{K\,s^{-1}}$.

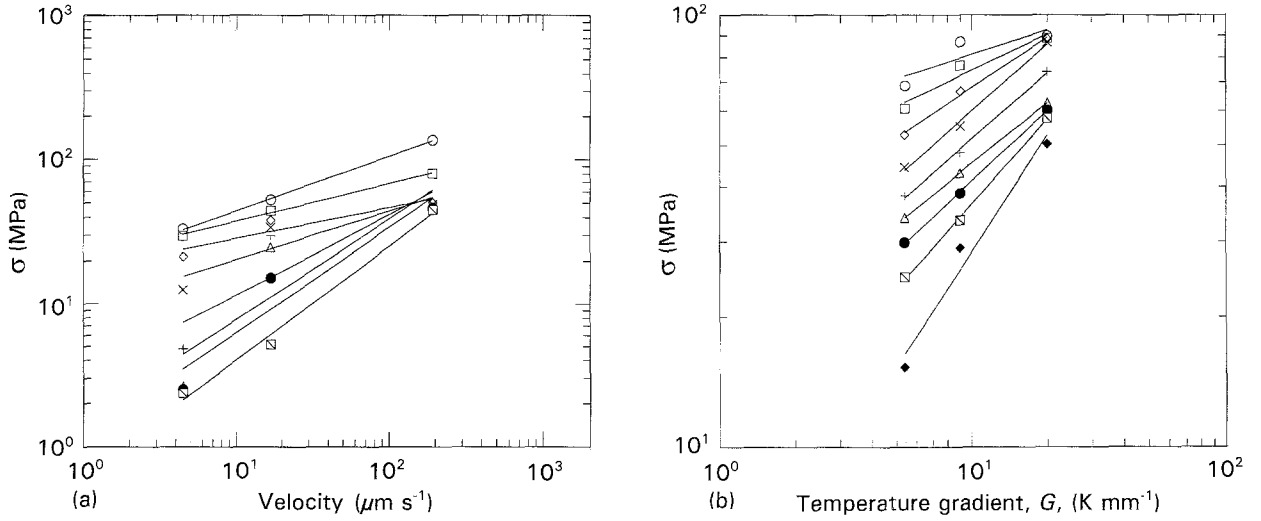

Figure 10 (a) The transverse stress at failure versus velocity for directionally solidified IC396M for temperature gradient $G = 5.4\ \mathrm{K\,mm^{-1}}$ and varying temperature: (○) 1350 K, (□) 1360 K, (◇) 1370 K, (×) 1380 K, (+) 1390 K, (△) 1400 K, (●) 1410 K, (⧅) 1420 K. (b) The transverse stress at failure versus temperature gradient, G, for directionally solidified IC396M at similar velocity ($V \sim 20\ \mu\mathrm{m\,s^{-1}}$), and varying temperatures: (○) 1330 K, (□) 1340 K, (◇) 1350 K, (×) 1360 K, (+) 1370 K, (△) 1380 K, (●) 1390 K, (⧅) 1400 K, (◆) 1410 K.

$T\varepsilon_{\mathrm{min\,f}}$, the amount of liquid was thick enough to collapse behind a growing crack, thus somewhat toughening the material. This process of reducing crack length as the crack propagates may lead to some of the solid taking up the load and manifesting in ductility. At very high temperatures, low ductility is once again observed and is related to the tearing of a predominantly liquid region.

The $T\varepsilon_{\mathrm{min\,f}}$ temperature is a function of the measurement type (i.e. transverse or longitudinal) and the solidification conditions. Three important temperatures are noted. These are ~ 1360, ~ 1420 and ~ 1460 K, which correspond to the $T\varepsilon_{\mathrm{min\,f}}$ for different conditions of imposed solidification: 1360 K is the $T\varepsilon_{\mathrm{min\,f}}$ for transverse testing when GV exceeds $0.1\ \mathrm{K\,s^{-1}}$; 1420 K is the temperature for transverse testing when GV is lower than $0.1\ \mathrm{K\,s^{-1}}$ and also longitudinal testing when GV exceeds $0.1\ \mathrm{K\,s^{-1}}$, 1460 K is the $T\varepsilon_{\mathrm{min\,f}}$ temperature for longitudinal testing in samples when GV is less than $0.1\ \mathrm{K\ s^{-1}}$. These may correspond to the critical film formation temperatures in the respective testing modes and to the upper hot tearing temperatures. Figs 7 and 8 show typical plots for the strain at failure at different temperatures for various solidification conditions and testing conditions.

The temperature at $\varepsilon_{\mathrm{min\,f}}$ (i.e. the minimum strain in the ε–T plot of Figs 7 and 8) is always higher for the longitudinal microstructure when compared with the corresponding transverse microstructure (Figs 7, 8). $\varepsilon_{\mathrm{min\,f}}$ is higher during longitudinal testing when compared to the corresponding transverse section.

The effect of the temperature gradient, G, and velocity, V, on the fracture stress in the transverse direction, σ_{T}, is to increase the fracture stress (Figs 10, 11). In the longitudinal direction, fracture stress, σ_{L}, decreases with the temperature gradient G (Table III).

The temperature bands in Fig. 12 correspond to the upper hot tearing temperatures and the critical film temperature. The arrows in Fig. 12 are from a sample

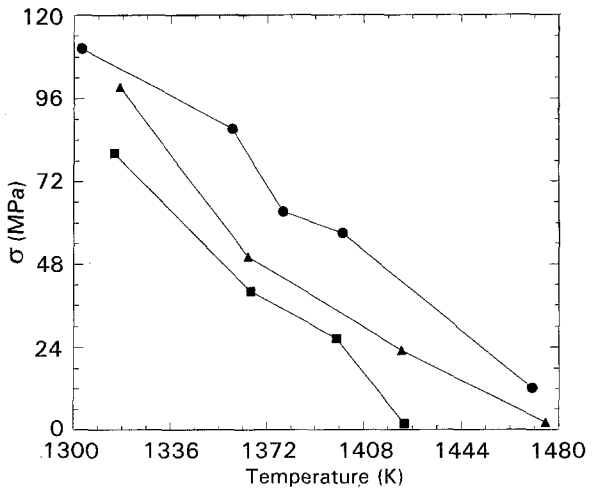

Figure 11 The transverse stress failure versus temperature for directionally solidified IC396M for similar velocity of solidification ($V \sim 20\ \mu m\ s^{-1}$) and varying temperature gradients: (●) 20 K mm^{-1}, (▲) 9 K mm^{-1}, (■) 5.4 K mm^{-1}.

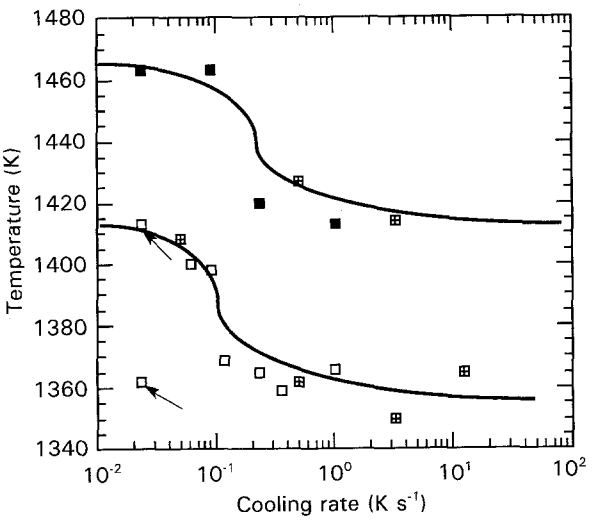

Figure 12 The temperature of $\varepsilon_{min\,f}$ versus cooling rate for the equiaxed and directionally solidified samples. The arrows point to samples with predominantly two-fold dendrites. (□) (DS) transverse, (■) (DS) longitudinal, (⊞) equiaxed.

which contained predominantly two-fold dendrites [2]. The two-fold dendritic structure has a predominantly cellular morphology [2]. The lower ductility minima temperature of this sample falls along the ductility minima band at the higher cooling rates of the transverse tested dendritic samples. The upper ductility minima for the two-fold dendrite samples corresponds to the upper hot tearing temperature.

3.3. Influence of microporosity, dendrite and grain parameters

An illustrative discussion on hot and residual cracking may be made from the fracture micrographs of the sample solidified at $V = 16.8\ \mu m\ s^{-1}$ and $G = 5.4$ K mm^{-1}. The longitudinal and transverse fracture stresses showed a monotonic decrease with increasing temperature. However, for the transverse microstructure, a minimum in the fracture strain was noted at an intermediate temperature (Figs 7, 8). The

TABLE III The longitudinal stress at failure at different temperatures for directionally solidified IC396M for similar velocity ($V \simeq 20\ \mu m\ s^{-1}$) of solidification and varying temperature gradients

Temperature (K)	σ_L (MPa)	
	$G = 5.4$ K mm^{-1}	$G = 9$ K mm^{-1}
1360	86.4	68.1
1370	86.2	61.5
1380	86.0	57.0
1390	85.1	50.1
1400	82.3	43.9
1410	72.2	37.3
1420	61.5	30.7
1430	51.8	25.5
1440	41.4	20.7
1450	30.7	15.5
1460	21.4	10.6

fractograph from the transverse tested samples always showed two types of region, A and B (Fig. 13). The equiaxed and longitudinal samples showed a more uniform fracture surface. Region A consisted of fine resolidified dendrites, whereas Region B consisted of decohesion fracture and plastic deformation of the original dendrites along with some resolidified liquid. For the transverse-tested samples, we note that fracture begins in the interdendritic region which first becomes liquid. This is Zone A. The crack may now transfer to an adjacent interdendritic region. Once this happens, this region is at a lower temperature and the propagation is now through a less liquid region, which is seen on the fracture surface as Zone B. This was verified from optical micrographs taken along the sample length after the fracture. The resolidified liquid in Region B was found to be mostly along the internal surface of the voids seen in Fig. 13c. The thin film described in Section 3.2 was always seen only in Region A. Fractographs of the longitudinally tested samples showed that, at high temperatures in the mushy region, decohesion was present along the primary dendrite arm boundaries but resolidified fine dendrites often filled voids that may have been created.

Note the resolidified dendrites, as well as regions of plastic tearing and decohesion. The relative proportion of the region of plastic deformation was noted to reduce with increasing temperature [6]. Decohesion started at the primary γ' and γ boundary which is the location of the microporosity (Fig. 14). This figure is taken at some distance behind the fracture surface. Note from previous work [2] that this microporosity increases with solidification velocity. Therefore, we may expect that the fracture strength measured longitudinally or transversely with increasing solidification velocity will show a decline. We note, however, that, relatively speaking, the longitudinal strength is insensitive to velocity as discussed above and also that, even though the porosity may increase, the strength is unaffected by porosity.

The transverse strength increases with solidification velocity. The microporosity seems to nucleate the crack that leads to fracture; however, the amount of

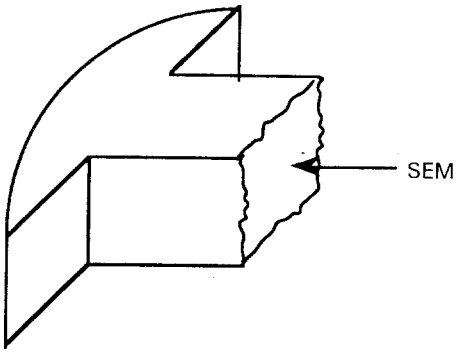

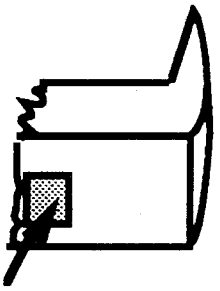

Metallography

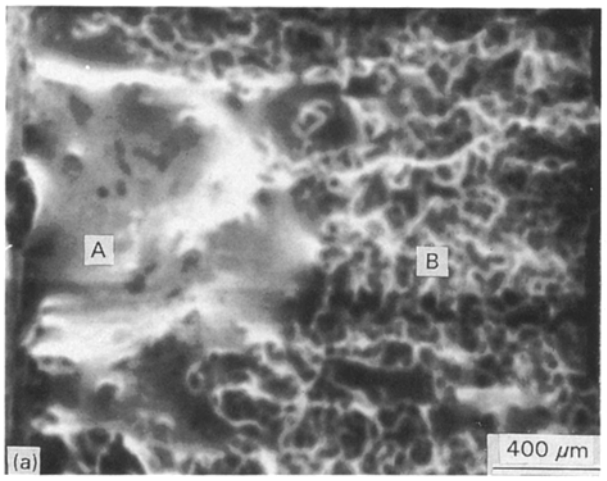

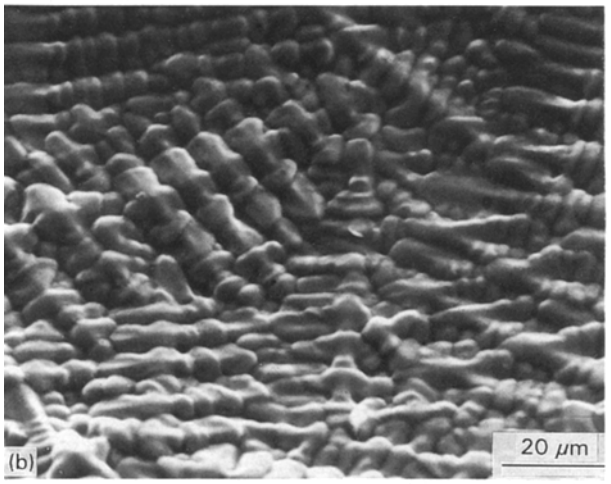

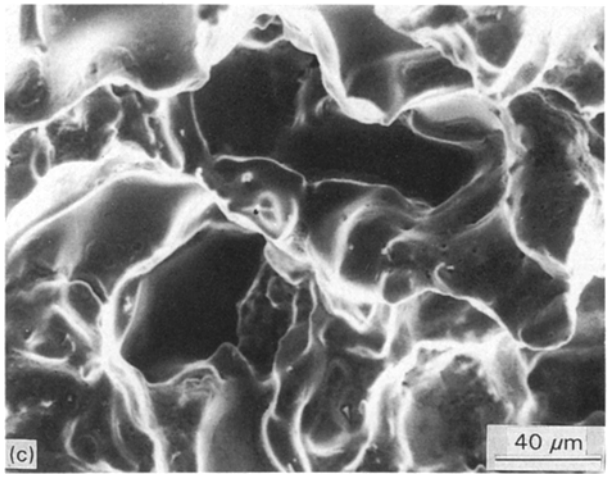

Figure 13 (a) The transverse scanning electron microscope fractograph of an elevated temperature fracture produced at 1470 K (in argon) for the directionally solidified bar at $G = 20\ \mathrm{K\,mm^{-1}}$ and $V = 17.9\ \mu\mathrm{m\,s^{-1}}$. (b, c) Magnified images of Regions A and B in (a), respectively.

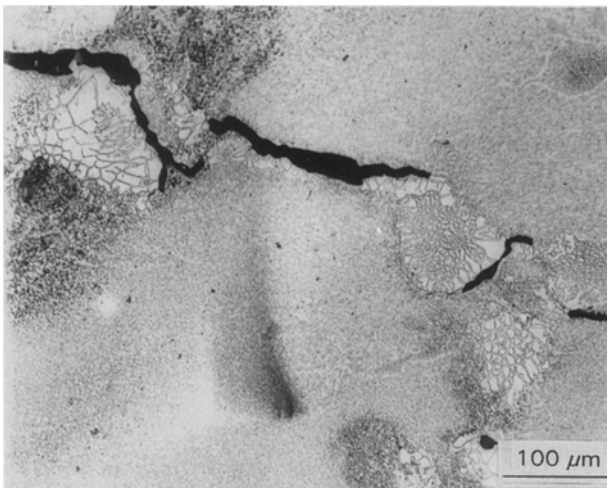

Figure 14 Metallographic cross-section perpendicular to the transverse fracture surface at 1375 K. Conditions of solidification are $G = 9\ \mathrm{K\,mm^{-1}}$, $V = 6.8\ \mu\mathrm{m\,s^{-1}}$.

this porosity within the bounds of the residual porosity seen in this alloy [2, 3] may not greatly influence the fracture strength. No simple relationship between microporosity and fracture strength is noted for directionally solidified samples [6]. For the equiaxed case, delamination is noted mostly at the grain boundaries. This is also the location of the macroporosity [7] which decreases (in size and volume) with the increase in cooling rate [6]. As the fracture strength decreases with increasing cooling rate, the macroporosity is expected to have a reduced influence on the fracture. The fracture stresses are dependent on the imposed velocity and temperature gradient during solidification. In the transverse case, as the gradient and velocity increase, an increase in the fracture stress is noted. In the longitudinal case, an increase in the temperature gradient during solidification causes the fracture stress to decrease. We note from previous work [2] that an increase in the temperature gradient and velocity will cause the secondary arm size to decrease. Note also from the discussion in Section 3.2 that a correlation between transverse strength and λ_2 is possible, but no correlation with λ_1 could be established.

When tested at temperatures below the strain minimum, no undue features were seen in the alloy microstructure behind the fracture surface. However, when tested at temperatures above the strain minimum, we noted residual cracking behind the fracture surface. These cracks could not be healed and would be left behind in a casting. Thus, a key result of the work is the identification of the intermediate temperature

strain minimum. If the casting experiences a temperature gradient during solidification and if the stresses are higher than the fracture stress at the temperature of the strain minimum, then residual tears will remain in the casting. This is the origin of one class of residual hot tears in an IC396M casting. Thus, during cooling, it is undesirable to have any stress at the temperature $T\varepsilon_{\min f}$. This is the temperature at which a very thin liquid film is present. Stresses cause a crack to propagate through this film. When the stresses cause the crack to grow to a critical length, failure occurs and very low ductility is observed. It is also entirely possible that even small stresses (not enough to cause failure) at this temperature will cause residual cracks in the casting (see Part I [1]).

For the generation of fracture maps, the cooling rate during directional solidification is not an appropriate variable as the fracture parameters do not scale monotonically with cooling rate. However, they do scale monotonically with plots of V and G plotted separately. The maps are presented in Section 3.5 below.

3.4. Hot tearing susceptibility

The hot tearing resistance is related to the amount of strain accommodation that is possible [8–20], although alternative definitions are available when lower fraction solids are considered [21, 22]. Lower grain sizes in equiaxed castings are known to be more resistant to hot tearing than the higher grain sizes [5, 8, 23–25]. This aspect has been discussed in Part I [1].

For directionally solidified samples, a higher fracture strain is noted for longitudinal testing than for transverse testing in the range of $\sim$1360–1420 K. When comparing transverse tested samples which were solidified at the same velocity but with different temperature gradients, it is noted that the fracture strain increases with increasing temperature gradient when the gradients are in the high range, $\sim$20 K mm^{-1}. In the lower range of 9 and 5.4 K mm^{-1}, the relationship is more complex and is dependent on the location of the temperature of the minimum ductility. An increase in the temperature gradient during solidification may cause a decrease in the fracture strain measured at the same temperature. Thus, there are two controlling parameters, the morphology and the microsegregation, for determining strain accommodation. The morphology being more important when cells and two-fold dendrites are present. Similarly for the transverse tested samples, solidified with the same gradient but with different velocities, the fracture strain is noted to increase with velocity. The influence of the velocity is smaller than that of the temperature gradient; the difference due to velocity becoming apparent only when comparing velocity changes over two orders of magnitude (e.g. 6 and 190 μm s^{-1}). If the velocity and temperature gradient both change the fracture strain in the same manner, the product of the two, namely the cooling rate, may influence the fracture strain (or the hot cracking resistance). However, this finding was not noted to be necessarily true because G and V may act in an opposing manner, thus cautioning against using a lumped variable, GV, instead of the individual variables.

For longitudinal testing, lowering the velocity increases the fracture strain. For the samples in the same velocity range, the higher temperature gradient gives higher strain accommodation. For the transverse samples in the same temperature gradient range, a higher velocity gives a higher strain accommodation. On the other hand, for the longitudinal samples, a lower velocity gives a higher strain accommodation prior to fracture. We note here also that a higher G is one of the causes of higher applied stress during solidification.

From Fig. 3 and Part I [1], we note that the upper hot tearing temperature for DS transverse tested and equiaxed samples increases with V, G, and decreases with $\dot{T}$, respectively (where $\dot{T}$ is the cooling rate for equiaxed samples). We note also that the hot tearing stresses are generally also expected to increase with V and G, and decrease with $\dot{T}$ respectively. The fracture strain dependence on V, G, and $\dot{T}$ is dependent on whether morphology control or microsegregation control dominates. For equiaxed castings, the decrease in the cooling rate, $\dot{T}$, and hence the increase in the coherency temperature, decreases the strain accommodation in the critical temperature range where tearing may occur. For the transverse DS samples, broadly speaking, the increase in the coherency temperature will decrease strain accommodation for dendritic samples but will increase strain accommodation for two-fold or cellular samples. The fracture strains were plotted against cooling rate for both the equiaxed samples and the transverse tested directionally solidified samples, to examine what would be expected in terms of hot cracking when a dendrite-to-equiaxed transition could occur. In general, it was noted that for the same cooling rates, when tested in the temperature range 1360–1420 K, the fracture strain in the equiaxed samples exceeded those in the DS samples. This would imply that a dendrite-to-equiaxed transition would increase the hot tearing resistance. Some exceptions were noted. These correspond to DS samples with predominantly two-fold dendrites (seen, for example, when the temperature gradient exceeded 20 K mm^{-1}). In such cases, the fracture strains for the equiaxed solidified samples were lower than the directionally solidified samples.

3.5. Fracture maps for nickel aluminide

Fracture maps may be defined as processing-property maps which may critically impact casting design. These maps should reflect conditions outside which the casting will tear. The fracture maps for IC396M have been developed after a critical examination of the solidified microstructure and the semi-solid strengths. The fracture maps are the $\sigma_T - T - G$ (transverse) for the directionally solidified microstructure and $\sigma_f - T - \dot{T}$ for equiaxed microstructure (Part I [1]). The $\sigma_T - T - G$ map is shown in Fig. 15. The $T\varepsilon_{\min f}$ band for the directionally solidified samples is also shown in the fracture map as this is the temperature at which residual microcracks may be left in the casting. The

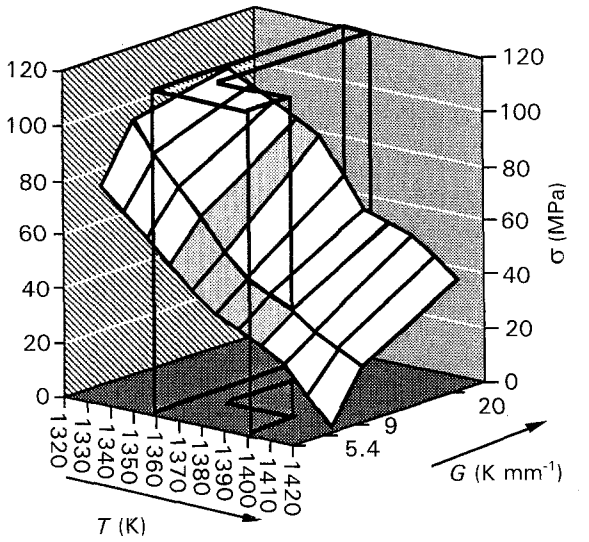

Figure 15 The three-dimensional diagram fracture map (transverse stress at fracture–temperature–temperature gradient) at a fixed velocity of $\sim 20\ \mu m\ s^{-1}$ for the directionally solidified IC-396M alloy. The shaded region is the temperature at which the minimum in the fracture strain was observed. At $G = 5.4\ K\ mm^{-1}$ the extended shaded region is shown to indicate the spread in this temperature with the velocity of solidification.

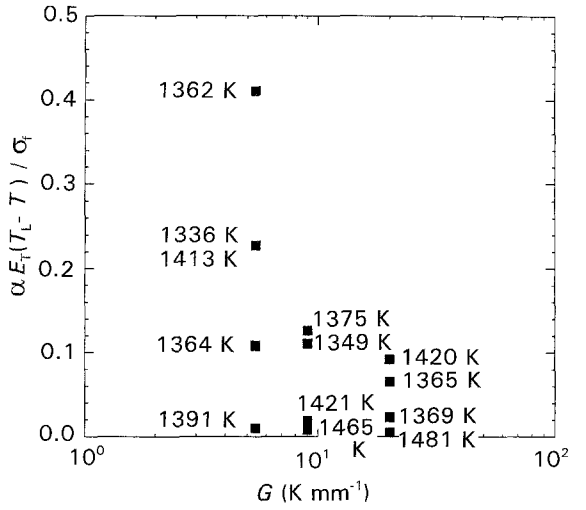

Figure 16 The ratio of imposed stress to the fracture stress at a given temperature versus temperature gradient for directionally soldified IC396M alloy at $V \sim 6\ \mu m\ s^{-1}$. α is taken as $13.6 \times 10^{-6}\ K^{-1}$ for the alloy; E_T is the measured modulus at a given temperature. T_L is the liquidus temperature. T is a given temperature. σ_f is the fracture stress at the same temperature.

band results from the finding that $T\varepsilon_{min\ f}$ is a function of the velocity of growth for the directionally solidified samples. The effect of the velocity on the extent of the band diminishes with an increase in the temperature gradient during solidification. In Part I it was noted that the volume fraction of γ' influences the modulus and thus the residual cracking found in castings after solidification. A similar analysis may be made for directionally solidified microstructures. The amount of γ' has been shown [1] to vary substantially with DS solidification conditions. The measured modulus at various temperatures below the film formation temperature may, therefore, be expected to be a function of the solidification condition. The ratio of imposed

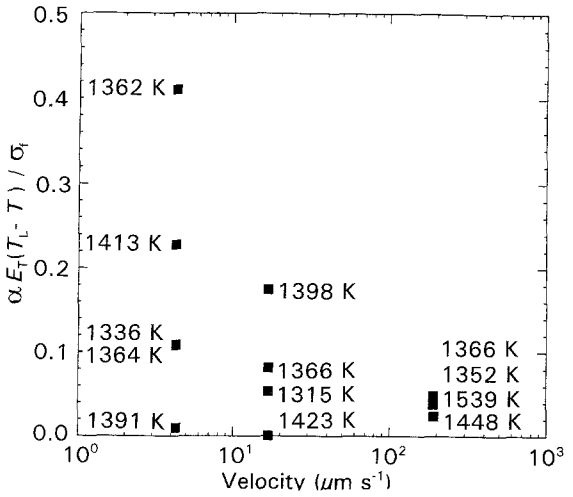

Figure 17 The ratio of imposed stress to the fracture stress at a given temperature versus velocity for directionally solidified IC396M alloy at $G = 5.4\ K\ mm^{-1}$. α is taken to be $13.6 \times 10^{-6}\ K^{-1}$ for the alloy; E_T is the measured modulus at a given temperature. T_L is the liquidus temperature. T is a given temperature. σ_f is the fracture stress at the same temperature.

stress to the fracture stress at a given temperature as a function of temperature gradient and velocity are plotted in Figs 16 and 17. The results are noted to follow very clearly the influence of the volume fraction of γ' measured from the microstructure [2] and as discussed in Part I [1].

4. Conclusions

This paper is the first report of systematic measurement of semi-solid stress–strain relationships for the directionally solidified alloys. The main conclusions of the work are given below.

The semi-solid strength, ductility and the upper hot tearing temperature are functions of the temperature and the solidified microstructure morphology. In general, the strength measured along the longitudinal direction of a directionally solidified sample is greater than that measured along the transverse direction, on account of a lack of solid continuity along the transverse direction. An analysis of the solidified microstructures indicates that finer secondary arm spacing increases the strength of the transverse microstructure. We conclude that, when considering processing maps for IC396M, the temperature gradient during solidification and the transverse direction properties limit the processing and therefore are the important variables.

There exists a critical temperature (for both DS and equiaxed samples) in the semi-solid region at which there is a strain minimum. This temperature is ~ 1360 K for cooling rates $> 0.1\ K\ s^{-1}$ in transverse DS or equiaxed tested samples. The temperature at $\varepsilon_{min\ f}$ (i.e. the minimum strain in the ε–T plot) and the $\varepsilon_{min\ f}$ is always higher for the longitudinal microstructure when compared with the corresponding transverse microstructure. The microstructural implication of the strain minimum are being examined. However, preliminary examination from fractographs indicate that the temperature is related to the formation of a thin

liquid film. The lower temperature of 1360 K is also the temperature at which residual microcracks may be left behind in the solidified structure.

Increasing V in transverse DS samples and $\dot{T}$ in equiaxed samples leads to an increase in the fracture strain and thus to an increase in the hot cracking resistance. The relationship with G in transverse DS samples is more complex. A dendrite-to-equiaxed transition is expected to increase the hot tearing resistance, except in special cases when two-fold dendrites are noted on directional solidification. Two-fold dendrites and/or cellular morphologies are noted when very high temperature gradients and low solidification velocities are imposed during solidification [2].

Fracture maps (processing maps) may be generated. These are the σ_T–T–G and σ_f–T–$\dot{T}$ maps for directional and equiaxed castings, respectively. The fracture map σ_T–T–G and σ_f–T–$\dot{T}$ may be used for design of castings. The solidification and cooling rates selected for this study (Parts I [1] and II) lie in the range of cooling rates commonly employed for commercial casting purposes. For a casting process we may obtain information on $\dot{T}$ or G during solidification. In addition, it is fairly simple to estimate the magnitude of mould-imposed stress on a casting [26–30]. By comparing the values with the σ_f–T–$\dot{T}$ plot, a determination may be made if there is any value that lies above the net. If a problem is anticipated, parameters like mould design, cooling rate, etc., may be changed to ascertain that there is no processing condition above the critical net. In addition, stresses at $T\varepsilon_{\min f}$ should be kept as low as possible to avoid residual microcracks.

It is important to mention two limitations of the present work. The first one is that the results obtained are from reheated samples and therefore may differ slightly from results obtained during *in situ* solidification measurement. Such differences have been recorded previously for other alloys [27, 31, 32]. The second is that the results also pertain to a single crosshead speed and therefore cover a small range of strain rates. Strain rate has sometimes been noted to influence the measured semi-solid properties (e.g. in snow [33] and in Pb–Sn alloys [27]). The strain rates that are estimated to be applied to the mushy zone during casting may vary over four orders of magnitude, i.e. 10^{-5}–10^{-1} s^{-1}. The results presented in this paper are for the higher strain rates (0.03–0.4 s^{-1}). Not withstanding these limitations, the results are the first comprehensive measurements which detail the semi-solid properties of a material as a function of the morphology and scale of the solidification microstructure in directionally solidified and equiaxed solidified alloys.

Acknowledgements

This work was performed as a part of a Edison Material Technology project CT-17 monitored by Drs E. F. Moore and L. Midolo. Dr Harold Gegel was task leader of the project. The alloys were obtained from Oak Ridge National Laboratory and ARMCO steel for which we thank Drs V. Sikka and R. O'Malley. The authors thank Professor K. Challenger for allowing us the use of the Gleeble Unit and for valuable discussions. Discussions with Dr A. Gokhale are also gratefully acknowledged.

References

1. C. S. LIN and J. A. SEKHAR, *J. Mater. Sci.* **28** (1993) 3581.
2. C. T. HO, C. J. CHENG and J. A. SEKHAR, *Metall. Trans.* **22A** (1991) 225.
3. C. J. CHENG and J. A. SEKHAR, in Materials Research Society Conference Proceeding on High Temperature Ordered Alloy", edited by L. A. Johnson, D. P. Pope and J. O. Stiegler, Vol. 213 (1991) p. 853.
4. V. K. SIKKA, *Mater. Manuf. Proc.* **4** (1989), 1.
5. J. C. BORLAND, *Brit Weld J.* **7** (1969) 508.
6. C. S. LIN, MS Thesis, University of Cincinnati (1990).
7. C. J. CHENG and J. A. SEKHAR, "Solidification Microporosity in IC396M: Nickel Aluminide", Vol. 2 Final report: Equiaxed Solidification, December 1990, Oak Ridge National Laboratory.
8. S. W. METZ and M. C. FLEMINGS, *AFS Trans.* **77** (1969) 329.
9. H. F. BISHOP, C. G. ACKERLAND and W. S. PELLINI, *ibid.* **65** (1957) 247.
10. A. COUTURE and J. O. EDWARDS, *ibid.* **81** (1973) 453.
11. W. S. PELLINI, *Foundry* November (1952) 125.
12. D. A. PINSKY, P. O. CHARREYRON and M. C. FLEMINGS, *Metall. Trans.* **15B** (1984) 173.
13. P. O. CHARREYRON and M. C. FLEMINGS, *Int. J. Mech. Sci.* **27** (1985) 781.
14. A. L. LUX and M. C. FLEMINGS, *Metall. Trans.* **10B** (1979) 71.
15. D. G. BACKMAN, R. MEHRABIAN and M. C. FLEMINGS, *ibid.* **8B** (1977) 471.
16. F. E. GOODWIN, P. DAVAMI and M. C. FLEMINGS, *ibid.* **11A** (1980) 1771.
17. T. MATSUMIYA and M. C. FLEMINGS, *ibid.* **12B** (1981) 17.
18. P. ACKERMANN, W. KURZ and W. HEINEMANN, *J. Mater. Sci. Engng* **75** (1985) 79.
19. C. M. SELLAR, *Int. Met. Rev.* **17** (1972) 1.
20. J. K. BRIMACOMBE, F. WEINBERG and E. B. HAWBOLT, *Metall. Trans. B* **10B** (1979) 279.
21. T. W. CLYNE and G. J. DAVIES, "Solidification and Casting of Metal" (The Metals Society, London, 1979) p. 275.
22. L. KATGERMAN, *Light Metals* (1980) 845.
23. J. C. BORLAND, *Brit Weld J.* **7** (1969) 508.
24. M. KUBOTA and S. KITAOKA, *AFS Trans.* **81** (1973) 424.
25. S. W. METZ and M. C. FLEMINGS, *ibid.* **78** (1970) 453.
26. M. C. FLEMINGS, "Solidification Processing" (McGraw-Hill, New York, 1975).
27. A. A. GOKHLE, *Trans. Ind. Inst. Metals* **39** (1986) 153.
28. A. ETIENNE and A. PALMERS, in "Solidification and Casting of Metal", (Metals Society, London, 1979) p. 295.
29. A. GRILL, J. K. BRIMACOMBE and F. WEINBERG, *J.ISI* **211** (1976) 34.
30. J. MATHEW and H. D. BRODY, "Solidification and Casting of Metal" (Metals Society, London, 1979) p. 244.
31. H. G. SUZUKI, S. NISHIMURA and S. YAMAGUCHI, *Trans. ISI Jpn* **22** (1982) 48.
32. K. KINOSHITA, G. KASAI and T. EMI, "Solidification and Casting of Metal", (Metals Society, London, 1979) p. 268.
33. H. NARITA, *J. Glaciology* **94** (1980) 275.

Received 2 June
and accepted 17 November 1992